

## Preparation and Characterization of Dy-doped Lithium Titanate ( $\text{Li}_4\text{Ti}_5\text{O}_{12}$ )

Keqiang Ding<sup>1\*</sup>, Jing Zhao<sup>1</sup>, Jinming Zhou<sup>1\*</sup>, Yongbo Zhao<sup>1</sup>, Yuying Chen<sup>1</sup>, Yan Zhang<sup>1</sup>, BinJuan Wei<sup>1</sup>, Li Wang<sup>2</sup>, Xiangming He<sup>2\*</sup>

<sup>1</sup>College of Chemistry and Materials Science Hebei Normal University, Shijiazhuang, Hebei 050024, P.R. China

<sup>2</sup>Institute of Nuclear & New Energy Technology, Beijing Key Lab of Fine Ceramics, Tsinghua University, Beijing 100084, China

\*E-mail: [dkeqiang@263.net](mailto:dkeqiang@263.net); [zhoujm@iccas.ac.cn](mailto:zhoujm@iccas.ac.cn); [hexm@tsinghua.edu.cn](mailto:hexm@tsinghua.edu.cn)

Received: 10 October 2015 / Accepted: 28 October 2015 / Published: 1 December 2015

---

For the first time, Dy (Dysprosium)-doped lithium titanate ( $\text{Li}_4\text{Ti}_5\text{O}_{12}$ , LTO) (denoted as Dy-LTO) was prepared by a sol-gel method assisted high temperature solid-state reaction, and the influence of Dy content on the electrochemical performance of LTO was thoroughly examined. The structure and morphology of the as-synthesized materials were mainly probed by X-ray diffraction (XRD) and scanning electron microscopy (SEM), and the electrochemical performance of the prepared samples was studied using cyclic voltammometry (CV), galvanostatic charge-discharge tests and electrochemical impedance spectroscopy (EIS) measurements. The obtained XRD patterns strongly demonstrated the formation of crystalline Dy-doped  $\text{Li}_4\text{Ti}_5\text{O}_{12}$ . SEM images indicated that when the atomic ratio of Dy to Ti was 0.06:4.94, some irregular smaller particles were found to be anchored on the surface of some huge particles. The results of electrochemical measurements revealed that  $\text{Li}_4\text{Ti}_{4.94}\text{Dy}_{0.06}\text{O}_{12}$  sample exhibited a specific capacity of  $145 \text{ mAh g}^{-1}$  after 20 cycles at a current rate of 0.5 C, which was much larger than that of pristine  $\text{Li}_4\text{Ti}_5\text{O}_{12}$  ( $104 \text{ mAh g}^{-1}$ ) and  $\text{Li}_4\text{Ti}_{4.8}\text{Dy}_{0.2}\text{O}_{12}$  ( $101 \text{ mAh g}^{-1}$ ).

---

**Keywords:** lithium titanate; Dysprosium doping; anode material; electrochemical performance

### 1. INTRODUCTION

Recently, rechargeable lithium ion batteries (LIBs) have attracted more and more attention mainly due to their high operating voltage, high energy density and low self-discharge rates [1]. However, some drawbacks, such as the limited cycling life and safety issue, still greatly prevent their further applications as next-generation power sources [1]. It is well known that except for cathode and electrolyte, the property of an anode material in LIBs is also a key parameter that could effectively

affect the electrochemical behavior of LIBs [2]. Although graphite has been widely employed as anode material in most commercial LIBs, the disadvantages of using graphite as anode material have been urgently addressed lately [3]. ( I ) The relatively lower theoretical capacity ( $372 \text{ mAh g}^{-1}$ ) of graphite substantially limited the power and energy density of a lithium-ion battery. ( II ) The potential for lithium intercalation in graphite is very close to the equilibrium potential of the  $\text{Li}^+/\text{Li}$  redox couple, thus, lithium plating may take place especially in the case of overcharging. The generated metallic lithium could result in the formation of Li dendrites, which may further produce short circuit and fire accidents [4]. ( III ) Due to the higher Fermi level of graphite anode, the electrolyte reduction reaction can take place at the interface between electrode and electrolyte, which would lead to the formation of SEI (solid electrolyte interphase ) layer during the first charge-discharge process. The formed SEI layer was detrimental to the capacity and power density as well as to the cycle-life [4]. ( IV ) During the full lithium insertion and extraction process the graphite anode undergoes a 9 vol.% variation, which may cause both the undesirable thickness change and mechanical degradation [5]. Therefore, exploiting novel anode materials of LIBs is still a major research topic in the research field of electrochemistry.

Of late, although many novel kinds of anode materials such as Si [6], Sn [7] and metal oxides like  $\text{SnO}_2$  [8],  $\text{Co}_3\text{O}_4$  [9] and NiO [10] have been prepared, lithium titanate was still paid much more attention due to its unique properties. Summarily, the following three features make LTO a promising anode material for LIBs. First, the voltage plateau of LTO (at around 1.55 V (vs.  $\text{Li}/\text{Li}^+$ )) was higher than the reduction potential of most cathode materials. Thus, some electrolyte decomposition reactions cannot happen, and thereby, the formation of SEI film could be well avoided [11]. Second, the volume expansion/contraction of LTO, that occurred in the lithiation/delithiation process, was much lower than that of graphite [11]. Thus, the LTO could exhibit better safety and cycling stability than the graphite.

However, recent works have revealed that the main disadvantage of using LTO is its low electronic conductivity ( $<10^{-13} \text{ S cm}^{-1}$ ), which may lead to poor capacity especially at high rates [12]. Numerous strategies have been developed to enhance the rate performance of LTO. These approaches mainly included nanostructuring LTO [13], coating LTO with cations [14], doping LTO with carbon or metals [15]. Among these developed methods, doping a metal into LTO to improve the electronic conductivity of LTO was regarded as a feasible approach owing to its simple manipulation and low-cost as compared to other methods. So far, many kinds of metals have been doped into LTO, showing an improved electrochemical performance. For example, Xiang's group [16] prepared Ce-doped  $\text{Li}_4\text{Ti}_5\text{O}_{12}$  anode materials via a solid state reaction, and found that  $\text{Li}_4\text{Ti}_5\text{Ce}_{0.1}\text{O}_{12}$  delivered the best rate performance among the pristine and Ce-doped  $\text{Li}_4\text{Ti}_5\text{O}_{12}$  materials. Guler et al. [17] synthesized spinel lithium titanates by a simple sol-gel method and then coated the surface of as-synthesized LTO powders with silver. He reported that the prepared Ag/LTO composite electrode displayed significantly improved high rate capability and stability compared to the pure LTO. Zhang et al. [18] systematically studied the influence of  $\text{Sc}^{3+}$  doping on the electrochemical performance of  $\text{Li}_4\text{Ti}_5\text{O}_{12}$  anode materials for lithium-ion battery, in which Sc-doped  $\text{Li}_4\text{Ti}_{4.95}\text{Sc}_{0.05}\text{O}_{12}$  was fabricated by a modified sol-gel method in the presence of chelating agent. Na-doped LTO was also prepared by Yi's group [19], and it was found that  $\text{Li}_{3.85}\text{Na}_{0.15}\text{Ti}_5\text{O}_{12}$  delivered better cycling performance relative to the pristine  $\text{Li}_4\text{Ti}_5\text{O}_{12}$ . Other metals, such as Mg [20] and V [21], were also doped into LTO to promote the

electrochemical performance of LTO. However, to the best of our knowledge, the preparation of Dy-doped LTO as anode materials for LIBs has not been reported so far.

In this work, Dy-doped LTO, namely,  $\text{Li}_4\text{Ti}_{5-x}\text{Dy}_x\text{O}_{12}$  ( $x=0, 0.06, 0.2$ , and the resultant samples were denoted as sample **a**, **b** and **c**, respectively.) was prepared for the first time by using a sol-gel method assisted high temperature solid-state reaction. It was found that  $\text{Li}_4\text{Ti}_{4.94}\text{Dy}_{0.06}\text{O}_{12}$  could deliver a specific capacity of  $145 \text{ mAh g}^{-1}$  after 20 cycles at a current rate of 0.5 C, which was much larger than that of pristine  $\text{Li}_4\text{Ti}_5\text{O}_{12}$  ( $104 \text{ mAh g}^{-1}$ ) and  $\text{Li}_4\text{Ti}_{4.8}\text{Dy}_{0.2}\text{O}_{12}$  ( $101 \text{ mAh g}^{-1}$ ).

## 2. EXPERIMENTAL

### 2.1. Materials

Tetrabutyl titanate ( $[\text{CH}_3(\text{CH}_2)_3\text{O}]_4\text{Ti}$ ), lithium acetate ( $\text{LiAc}\cdot 2\text{H}_2\text{O}$ ) and  $\text{Dy}_2\text{O}_3$  were all purchased from Tianjin Chemical Reagent Co. Ltd. All materials used in the electrochemical measurement, like polytetrafluoroethylene (PTFE) binder, acetylene black, electrolyte of 1 M  $\text{LiClO}_4$  and the cell, were all bought from Tianjin Lianghuo S&T Developing Co. Ltd. Except where specified, all the chemicals were used as-received without any further treatment.

### 2.2. Preparation of $\text{Li}_4\text{Ti}_{5-x}\text{Dy}_x\text{O}_{12}$

Firstly, a proper amount of  $\text{LiAc}\cdot 2\text{H}_2\text{O}$  and  $\text{Dy}_2\text{O}_3$  were dissolved in doubly-distilled water to form solution **1**, and meanwhile, a proper volume of  $[\text{CH}_3(\text{CH}_2)_3\text{O}]_4\text{Ti}$  was dropped into a amount of anhydrous alcohol to form solution **2**. And then, solution **2** was transferred into solution **1** dropwise under vigorously stirring, leading to the formation of a milky colloid. Subsequently, the resulting colloid was dried in an air dry oven at  $150 \text{ }^\circ\text{C}$  for 3 h generating a precursor. And these obtained precursors were thoroughly ground in an agate mortar for 30 min, and after that the prepared powders were pressed into tablets by a bead machine. Lastly, the resulting tablets were sintered in a muffle furnace under air conditions at  $800 \text{ }^\circ\text{C}$  for 10 h to produce the samples. It should be noted that the amounts of  $\text{LiAc}\cdot 2\text{H}_2\text{O}$  and  $\text{Dy}_2\text{O}_3$  and  $[\text{CH}_3(\text{CH}_2)_3\text{O}]_4\text{Ti}$  were determined by the molecular formula of  $\text{Li}_4\text{Ti}_{5-x}\text{Dy}_x\text{O}_{12}$ . The samples with  $x$  values of 0, 0.06 and 0.2 were denoted as sample **a**, **b** and **c**, respectively.

### 2.3. Characterization

Scanning electron microscopy (HITACHI, SEM S-570) was employed to characterize the particle morphology. X-ray diffraction (Bruker AXS, D8 ADVANCE, Germany) was used to identify the crystal structure of the obtained samples. The components of the as-prepared samples were analyzed by energy dispersive spectrometer (EDS, INCA Energy 350, England). Fourier transform infrared spectrometry (FT-IR) measurements were carried out on a Hitachi FT-IR-8900 spectrometer (Japan).

All electrochemical measurements such as cyclic voltammetry (CV) and electrochemical impedance spectroscopy (EIS) were performed on a personal computer-controlled CHI 660B electrochemical workstation (Shanghai Chenhua Apparatus, China). The amplitude and frequency ranges of alternating current employed were 5 mV and 100 kHz-0.1 Hz in the EIS measurements, respectively. All the experiments were conducted at room temperature.

#### 2.4. Preparation of working electrodes

The typical process for preparing a working electrode was described as follows. Firstly, the resulting active material powders, acetylene black and polyvinylidene fluoride were totally mixed in an agate mortar at a weight ratio of 80:10:10 for about 30 min, and then the mixture was blended by using NMP(N-methylpyrrolidone) as the binder to produce a kind of slurry. Subsequently, the obtained slurry was pasted onto an Al foil by a clean glass piece, followed by drying at 120 °C for 6 h in a vacuum oven. Two-electrode electrochemical cells were assembled in a high pure nitrogen-filled glove box. The two-electrode electrochemical cell included a lithium metal foil, Celgard 2400 separator, and an electrolyte of 1 M LiClO<sub>4</sub>. It should be mentioned that the solvent of the electrolyte was a mixed solvent that contained ethylene carbonate (EC) and diethyl carbonate (DEC) and dimethyl carbonate (DMC) (EC:DEC:DMC=2:5:11, in volume). Evidently, metallic lithium foils were utilized as not only reference electrode but also counter electrodes. A battery testing system (CT-3008W-5V20mA-S4, Shenzhen Neware Electronics Co., Ltd. China) was employed to complete the battery measurements. The potential range of charge-discharge testing was from 0.5 V to 2.5 V, and various current rates ( 1C=175mAh g<sup>-1</sup>, 0.5C、 1C、 1.5C and 2C were employed ) were applied to the cells to evaluate the rate performance of active materials.

### 3. RESULTS AND DISCUSSION

#### 3.1 XRD analysis

XRD patterns for the as-synthesized samples as well as the standard XRD pattern of Li<sub>4</sub>Ti<sub>5</sub>O<sub>12</sub> are all presented in Fig.1. Apparently, for all the three samples, six characteristic diffraction peaks corresponding to LTO were clearly displayed in Fig.1. Namely, the diffraction peaks positioned at 18.5°, 35.8°, 43.4°, 57.5°, 63.0° and 66.1° could be well indexed as the (111), (311), (400), (333) , (440) and (531) crystal planes of Li<sub>4</sub>Ti<sub>5</sub>O<sub>12</sub> (JCPDS no. 00-049-0207), respectively [15]. It substantially indicated the formation of LTO. Also, this result implied that the main crystal structure of LTO was not destroyed by the doped Dy. Although the main typical reflections of LTO were all displayed in the XRD patterns of the three samples, the intensities of these peaks were different from each other. Generally, a higher diffraction peak corresponded to a higher crystallinity of a product. Thus, it can be concluded that sample **a** showed the best crystallinity among all the samples. Additionally, the diffraction peaks belonging to TiO<sub>2</sub> were distinctly exhibited in the XRD patterns of the three samples. It indicated that TiO<sub>2</sub> as impurity existed in the resulting products. Interestingly, for

sample **c**, a novel diffraction peak centered at  $15.7^\circ$  appeared clearly, indicative of the presence of  $\text{Li}_2\text{Ti}_4\text{O}_9$ .

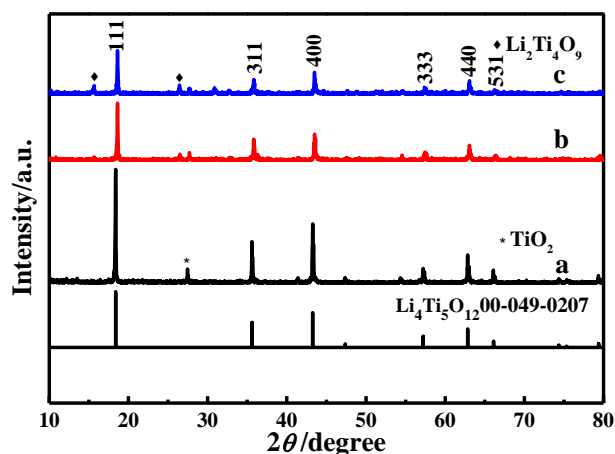


**Figure 1.** XRD patterns for the prepared samples. Pattern **a**, **b** and **c** corresponded to sample **a**, **b** and **c**.

The average crystallite sizes for sample **a**, **b**, and **c** were calculated using Scherrer's equation [22] from (400) facet to be 143 nm, 109 nm and 118 nm, respectively. Unfortunately, the particle sizes estimated directly from the SEM images were larger than these crystallite sizes calculated from XRD patterns. After the careful observation of Fig.1, two conclusions can be achieved. (1) The doped Dy did not destroy the main crystal structure of LTO; (2) As the atomic ratio of Ti to Dy was 4.8:0.2, the crystallinity of LTO became poor and some impurities appeared in the prepared samples.

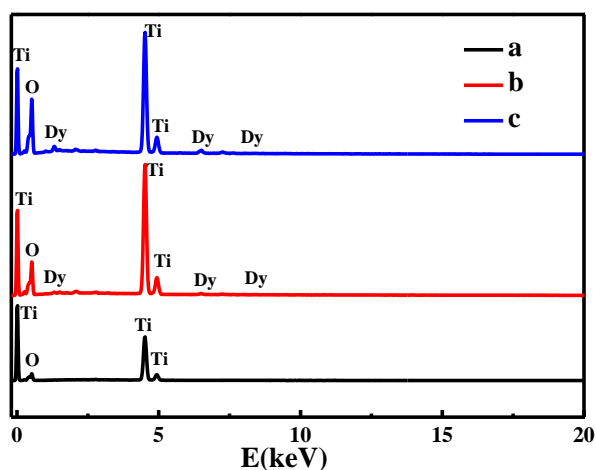


**Figure 2.** EDS spectra for the prepared samples. Spectrum **a**, **b** and **c** corresponded to sample **a**, **b** and **c**.

The results of EDS analysis for the three samples are plotted in Fig.2. As indicated from the result, the elements of O, Ti and Dy were well-distributed in the Dy-doped LTO, which effectively demonstrated that Dy as a doper has been successfully doped into the resultant samples. Theoretically, the atomic ratio of O to Ti was equal to 2.4 for a pure LTO. Nevertheless, the atomic ratios of O to Ti

were 2.28, 2.01 and 2.08 for sample **a**, **b** and **c**, respectively. That is to say, the atomic ratios of O to Ti for the three samples were much lower than that of the theoretical value. It suggested that some impurities were formed in the resulting samples, which was consistent with the results of XRD pattern (Fig.1). Also, above results effectively demonstrated that the developed method of sol-gel assisted high temperature solid-state method was a feasible way to fabricate crystalline LTO though some impurities were contained in the resultant samples.

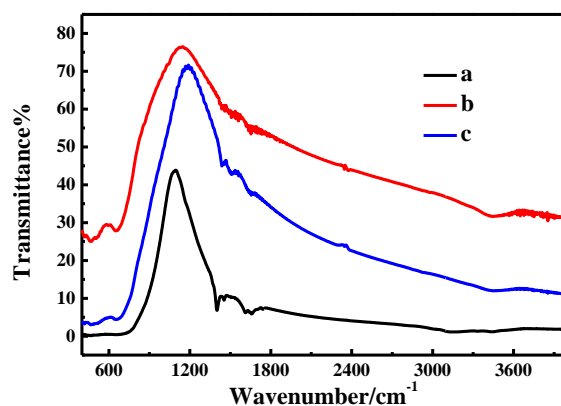


**Figure 3.** FT-IR spectra for the prepared samples. Spectrum a, b and c corresponded to sample **a**, **b** and **c**.

FT-IR spectra for the prepared materials are shown in Fig. 3. According to the previous reports on LTO [23, 24], the weak absorption peak at  $2355\text{ cm}^{-1}$  should be assigned to the stretching vibration of Ti-O bond, and the absorption bands appearing at  $668.3\text{ cm}^{-1}$  were resulted from the  $\text{MO}_6$  ( $\text{TiO}_6$ ) octahedron. The bands at  $1622.0\text{ cm}^{-1}$  and  $3429.2\text{ cm}^{-1}$  should correspond to the C=O and -OH groups, respectively. It was proposed that these two peaks were originated from the strong absorption of  $\text{CO}_2$  and  $\text{H}_2\text{O}$  on LTO material in the air. Thus, FT-IR spectra further demonstrated that the major groups of LTO were all contained in the Dy-doped LTO.

### 3.2 Morphology characterization

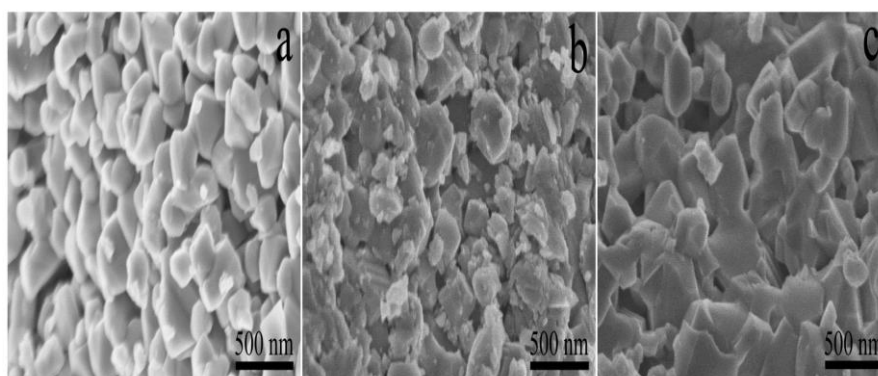


**Figure 4.** SEM images for the prepared samples. Image a, b and c corresponded to sample **a**, **b** and **c**.

To better observe the morphology of the obtained samples, SEM measurements were performed and the corresponding SEM images are provided in Fig.4. The average particle sizes for sample **a**, **b** and **c** were estimated to be 270 nm, 208 nm and 458 nm, respectively. Therefore, sample **b** showed the smallest particle size among all the samples. Generally, the smaller particle size would increase the contacting area between the electrolyte and electrode, and would decrease the diffusion path length of Li ions, showing positive effect for an anode material. Apparently, the particles of sample **a** and **c** have more regular crystal structure as compared to sample **b**. Also, the particle size distribution of sample **a** and **c** was more uniform than that of sample **b**. It can be seen from image **b** that some smaller pulverized particles were embedded into huge particles. This peculiar structure of sample **b**, probably, could reduce the mechanical strain of particles that was originated from the volume change in the extraction/insertion process of Li-ions, leading to an improved electrochemical performance. Additionally, the irregular crystal structure of sample **b** would generate a large number of “crystal defects”, which would further produce many “vacancy defects”. A proper amount of vacancy defects could play a key role in electronic conductivity enhancement of an electrode material [25].

### 3.3 Electrochemical properties

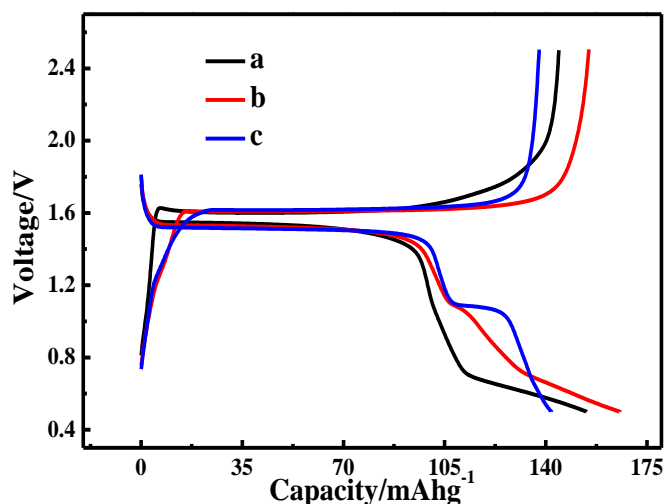


**Figure 5.** Charging-discharging profiles for the prepared cells obtained at 0.5C. Curves a, b and c corresponded to sample **a**, **b** and **c**.

The first charge-discharge curves recorded in the potential range of 0.5-2.5 V at the current rate of 0.5C are illustrated in Fig.5. The voltage plateaus appearing at around 1.60V and 1.55V corresponded to charging and discharging process, respectively. This result was consistent with the previous studying very well [26]. The presence of voltage plateau in the charge-discharge curves, generally, indicated the occurring of a phase transition process [27]. Surprisingly, in the case of sample **c**, two voltage plateaus were displayed clearly in the discharging profiles, suggesting a two step Li-ion intercalation process was involved. The initial discharge capacities were evaluated to be 154, 164 and 142 mAh g<sup>-1</sup>, respectively, for sample **a**, **b** and **c**. It illustrated that sample **b** displayed the largest

value of specific capacity among all the materials, which was probably attributed to its relatively smaller average particle size and its particular structure as compared to other samples. The smaller particle size may shorten the diffusion path of Li-ions, which was beneficial to the extraction/insertion process of Li-ions. Meanwhile, the peculiar structure of sample **b** possibly could reduce some mechanical strains that were originated from the volume variations during delithiation-lithiation process.

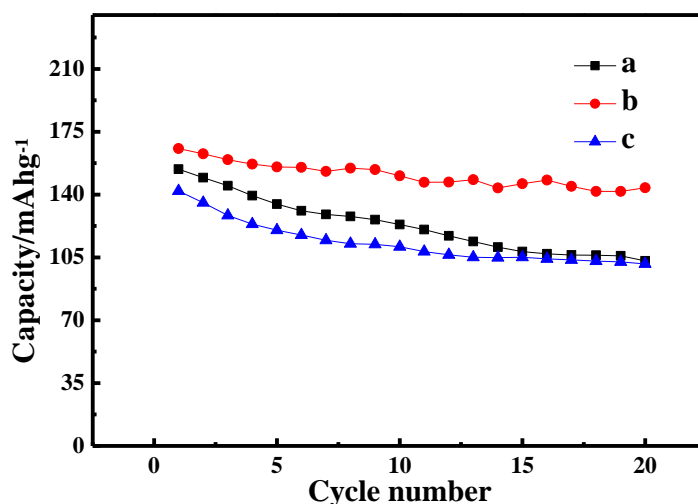


**Figure 6.** Cycle performance of the prepared electrodes at 0.5C rate, line a, b and c corresponded to sample **a**, **b** and **c**.

Fig. 6 showed the comparison in cycling performance for all the prepared electrodes. As can be observed, the discharge capacities for all electrodes decreased steadily with increasing the cycling number, which was ordinarily resulted from the irreversibility of a practical cell.

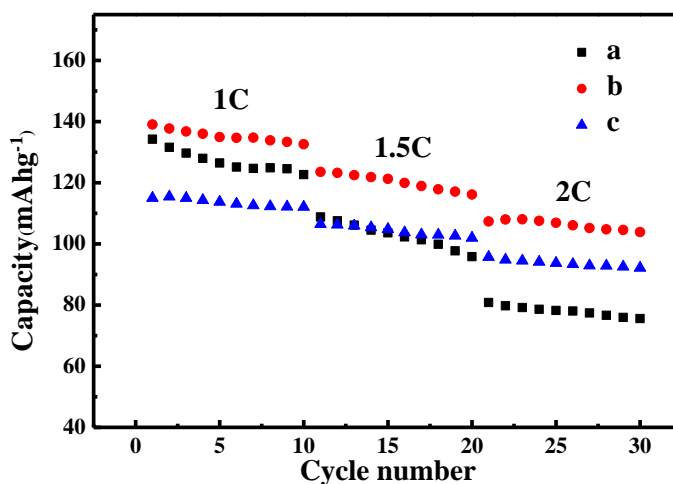


**Figure 7.** Comparison of the rate capabilities of all the prepared electrodes, line a, b and c corresponded to sample **a**, **b** and **c**.

However, close observation revealed that the capacity fading rates were different from each other. For instance, after 20 cycles, the capacity dropped from 154 to 104, 164 to 144, and 142 to 102 mAh g<sup>-1</sup> for sample **a**, **b** and **c**, respectively. The capacity retention efficiencies for sample **a**, **b** and **c** were about 67.5%, 87.8% and 71.8%, respectively. Thus, sample **b** showed both the highest value of specific capacity and the largest capacity retention among all the samples.

To estimate the rate capability of the as-synthesized working electrodes, various current rates were applied to the sample-assembled cells in order to plot the curve of capacity against cycling number. Each rate tests were conducted for 10 cycles, and the results were given in Fig.7. Evidently, the cell that was constructed by sample **b** delivered the largest discharge capacity in all the rate measurements, though the values of discharge capacity dropped evidently with increasing the current rate. This indicated that sample **b** had better rate capability than other samples.

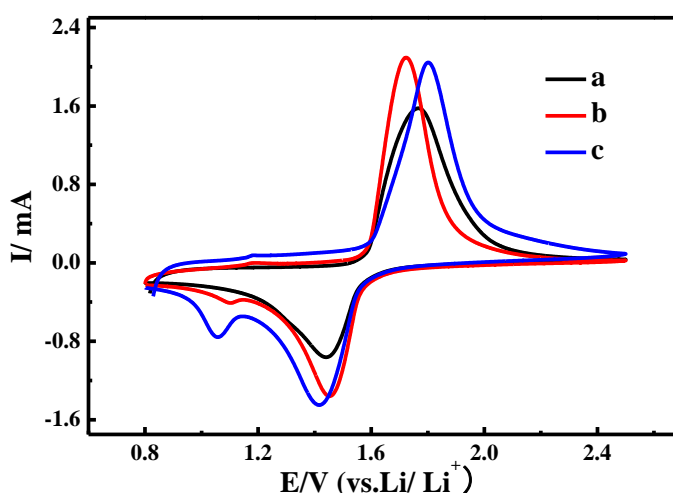


**Figure 8.** Cyclic voltammograms (CVs) for as-prepared electrodes at a scan rate of 0.5 mV s<sup>-1</sup>. Curve a, b and c corresponded to sample **a**, **b** and **c**.

To further study the delithiation-lithiation performance of the prepared working electrodes, cyclic voltammetry (CV) measurements were conducted and the CV curves obtained at the scanning rate of 0.5 mV s<sup>-1</sup> are plotted in Fig. 8. In the anodic potential scanning, for all the electrodes, one sharp oxidation peak positioned at around 1.7 V was displayed, which should be assigned to the delithiation process of Li ions from Li<sub>4</sub>Ti<sub>5-x</sub>Dy<sub>x</sub>O<sub>12</sub>. Interestingly, in the cathodic potential scanning, one reduction peak centered at about 1.4 V was observed for the pure LTO (curve a), while, for the Dy-doped samples, except for the main peak located at about 1.4 V, one small peak at 1.0 V was distinctly displayed. In general, the oxidation (anodic) peaks in CV curves corresponded to the deintercalation process of Li-ion, and the reduction (cathodic) peaks were associated with the intercalation process of Li-ion [28]. Thus, Dy-doped LTO had two steps of intercalation process for Li-ions, which was consistent with the fact that two voltage plateaus were observed in the discharging curves of sample **b** and **c** (Fig.5). To the best of our knowledge, this is the first time to report the small reduction peak of metal-doped LTO at about 1.0V though many CV curves of metal-doped LTO have been published in

the previous studies. That is to say, some unknown interactions between Dy and LTO really existed which required further investigation.

Additionally, both the anodic and cathodic peak currents were all drastically increased for the Dy-doped LTO as compared to the pure LTO. It suggested that the Li-ion and electron kinetics of Dy-doped LTO was faster than that of the pure LTO. According to our previous works [29], the potential interval ( $\Delta E_p = E_{pa} - E_{pc}$ ) could be used as a parameter to reflect the reversibility of an electrochemical reaction. The smaller the value of  $\Delta E_p$  is, the more reversible the electrochemical reaction will be. The potential intervals for sample **a**, **b** and **c** were 330 mV, 280 mV and 390 mV, respectively. Therefore, sample **b** delivered the best reversibility among all the samples, which could well explain the fact that sample **b** exhibited the best cycling stability in comparison with other two samples.

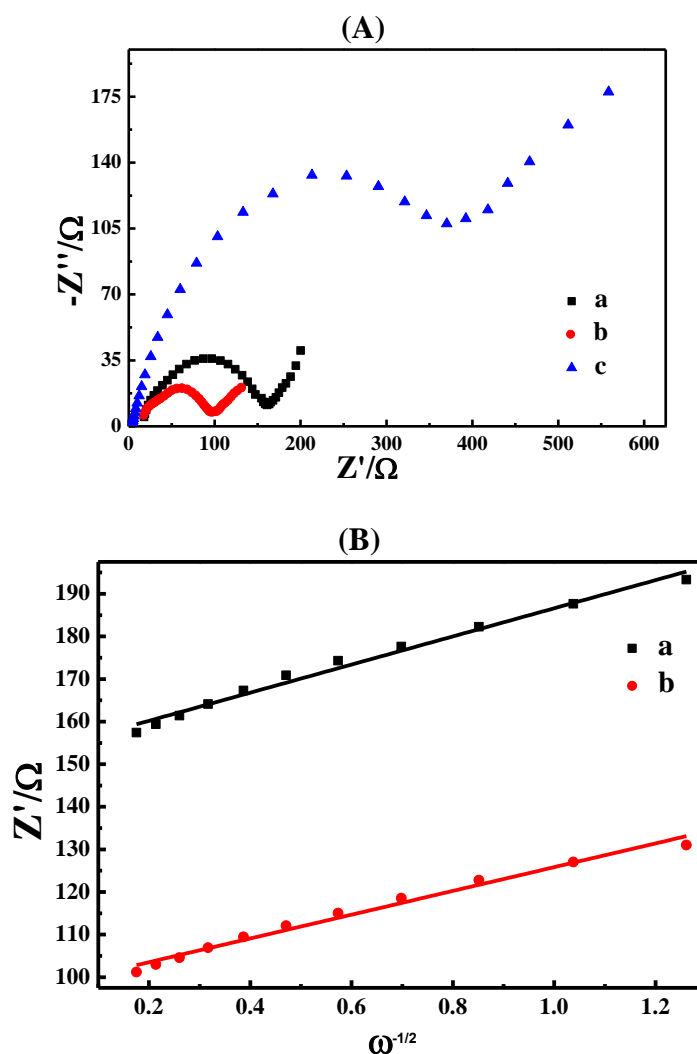


**Figure 9.** (A) Nyquist plots spectra obtained at the open circuit potentials for all the prepared electrodes within the frequency range of 100 kHz to 0.1 Hz. Spectra a, b and c corresponded to sample **a**, **b** and **c**. (B) Curves of  $Z'$  plotted against  $\omega^{-1/2}$  at low frequency region for the pristine LTO and the  $\text{Li}_4\text{Ti}_{4.94}\text{Dy}_{0.06}\text{O}_{12}$ .

To study Li-ion and electron kinetics in the as-prepared working electrodes, electrochemical impedance spectroscopy (EIS) measurements were carried out at the open circuit potential. The Nyquist plots for the three kinds of cells are illustrated in Fig. 9 (A). Apparently, all the curves displayed a semi-circle in the high-frequency region and an inclined straight line in the low-frequency region. Generally, the value of the diameter for the semi-circle was directly related to charge-transfer resistance ( $R_{ct}$ ) at the electrode|electrolyte interface, and a larger semi-circle corresponded to a bigger value of  $R_{ct}$ . The straight line appearing in the low frequency region was originated from a solid-state diffusion-controlled process of Li-ion [15, 27]. The values of  $R_{ct}$  for sample **a**, **b** and **c** were estimated to be 169.4  $\Omega$ , 99.5  $\Omega$ , 504.2  $\Omega$ , respectively. Thus, sample **b** delivered the smallest value of  $R_{ct}$  among all the samples. It implied that sample **b** had faster lithium insertion/extraction kinetics as compared to other samples, which may account for the largest discharge capacities and best cycling stability of sample **b** when compared to sample **a** and **c**.

According to the previous report [30], Li-ion diffusion coefficient in the materials could also be determined by using the relationship between the low frequency Warburg impedance and their corresponding angular frequencies according to the following equations.

$$Z_{re} = R_s + R_{ct} + \sigma_m \omega^{-1/2} \quad (1)$$

Where  $Z_{re}$  is the real part of the impedance;  $R_s$  the resistance of electrolyte;  $R_{ct}$  the charge transfer resistance and  $\omega$  is the angular frequency in the low frequency region. The typical curve of  $Z_{re}$  vs. the reciprocal root square of the lower angular frequencies ( $\omega^{-1/2}$ ) for pure LTO and  $\text{Li}_4\text{Ti}_{4.94}\text{Dy}_{0.06}\text{O}_{12}$  is shown in Fig. 9 (B), thus, the value of  $\sigma_m$  could be obtained directly. And then, the lithium ion diffusion coefficient can be calculated from the formula as follows [31]:

$$D_{Li} = \frac{1}{2} \left[ \left( \frac{V_m}{AF \sigma_m} \right) \frac{dE}{dx} \right]^2 \quad (2)$$

Where  $V_m$  is the molar volume of  $\text{Li}_4\text{Ti}_5\text{O}_{12}$  ( $45.73 \text{ cm}^3 \text{ mol}^{-1}$ ),  $F$  Faraday constant,  $A$  the total contact area between the electrolyte and the electrode,  $dE/dx$  is the slope of the open-circuit voltage versus mobile  $\text{Li}^+$  concentration  $x$ . The calculated lithium diffusion coefficient  $D_{\text{Li}^+}$  of the sample **b** was  $11.01 \times 10^{-10} \text{ cm}^2/\text{s}$ , larger than the pristine LTO ( $8.08 \times 10^{-10} \text{ cm}^2/\text{s}$ ). It strongly demonstrated that the lithium ion mobility in the pure LTO could be effectively augmented by the doped Dy. Thus, the electrochemical behavior of pure LTO could be drastically improved with a proper amount of doped Dy.

#### 4. CONCLUSIONS

For the first time, Dy-doped LTO particles with well-defined crystal structure were prepared by a sol-gel assisted high temperature solid-state method under the air conditions. The effect of Dy-doping content on the electrochemical performance of the as-synthesized samples was preliminarily investigated. XRD analysis indicated that the main crystal structure of LTO was not destroyed by the doped Dy though the crystallinity of the produced samples became poor as the content of Dy was increased. When the atomic ratio of Dy to Ti was 0.06:4.94, some irregular smaller particles were

found to be embedded into some huge particles. The results of electrochemical measurements revealed that  $\text{Li}_4\text{Ti}_{4.94}\text{Dy}_{0.06}\text{O}_{12}$  sample exhibited the largest specific capacity and best rate capability among all the prepared electrodes.

#### ACKNOWLEDGEMENTS

This work was financially supported by the National Natural Science Foundation of China (No. 21173066 and 21403052), Natural Science Foundation of Hebei Province of China (No. B2011205014, B2015205150 and 2015205227).

#### References

1. L. Croguennec and M. Rosa Palacin, *J. Am. Chem. Soc.*, 137 (2015) 3140.
2. D. Pham-Cong, J.-H. Kim, S.-Y. Jeong, J. H. Choi, J. Kim and C.-R. Cho, *Electrochem. Commun.*, 60 (2015) 204.
3. D. Sun, M. Wang, Z. Li, G. Fan, L.-Z. Fan and A. Zhou, *Electrochem. Commun.*, 47 (2014) 80.
4. H. Ming, J. Ming, X. Li, Q. Zhou, H. Wang, L. Jin, Y. Fu, J. Adkins and J. Zheng, *Electrochim. Acta*, 116 (2014) 224.
5. C. Cheng, H. Liu, X. Xue, H. Cao and L. Shi, *Electrochim. Acta*, 120 (2014) 226.
6. J. L. Gómez-Cámer, H. Thuv and P. Novák, *J. Power Sources*, 294 (2015) 128.
7. M. Lübke, I. Johnson, N. M. Makwana, D. Brett, P. Shearing, Z. Liu and J. A. Darr, *J. Power Sources*, 294 (2015) 94.
8. W. Li, D. Yoon, J. Hwang, W. Chang and J. Kim, *J. Power Sources*, 293 (2015) 1024.
9. Y. Wang, B. Wang, F. Xiao, Z. Huang, Y. Wang, C. Richardson, Z. Chen, L. Jiao and H. Yuan, *J. Power Sources*, 298 (2015) 203.
10. N. S. Spinner, A. Palmieri, N. Beauregard, L. Zhang, J. Campanella and W. E. Mustain, *J. Power Sources*, 276 (2015) 46.
11. T.-F. Yia, S.-Y. Yang, M. Tao, Y. Xie, Y.-R. Zhu and R.-S. Zhu, *Electrochim. Acta*, 134 (2014) 377.
12. Y.-Q. Wang, L. Gu, Y.-G. Guo, H. Li, X.-Q. He, S. Tsukimoto, Y. Ikuhara and L.-J. Wan, *J. Am. Chem. Soc.*, 134 (2012) 7874.
13. W. Zhang, J. Li, Y. Guan, Y. Jin, W. Zhu, X. Guo and X. Qiu, *J. Power Sources*, 243 (2013) 661.
14. B. Zhang, Z.-D. Huang, S.W. Oh and J.-K. Kim, *J. Power Sources*, 196 (2011) 10692.
15. N. Li, J. Liang, D. Wei, Y. Zhu and Y. Qian, *Electrochim. Acta*, 123 (2014) 346.
16. T.P. Zhou, X.Y. Feng, X. Guo, W.W. Wu, S. Cheng and H.F. Xiang, *Electrochim. Acta*, 174 (2015) 369.
17. A. Erdas, S. Ozcan, D. Nalci, M. O. Guler and H. Akbulut, *Surf. Coat. Tech.*, 271 (2015) 136.
18. Y. Zhang, C. Zhang, Y. Lin, D.-B. Xiong, D. Wang, X. Wu and D. He, *J. Power Sources*, 250 (2014) 50.
19. T.-F. Yi, S.-Y. Yang, X.-Y. Li, J.-H. Yao, Y.-R. Zhu and R.-S. Zhu, *J. Power Sources*, 246 (2014) 505.
20. W. Wang, B. Jiang, W. Xiong, Z. Wang and S. Jiao, *Electrochim. Acta*, 114 (2013) 198.
21. T.-F. Yi, J. Shu, Y.-R. Zhu, X.-D. Zhu, C.-B. Yue, A.-N. Zhou and R.-S. Zhu, *Electrochim. Acta*, 54 (2009) 7464.
22. K. Ding, Y. Zhao, L. Liu, Y. Cao, Q. Wang, H. Gu, X. Yan and Z. Guo, *Int. J. Hydrogen. Energ.*, 39 (2014) 17622.
23. F. Wu, Z. Wang, X. Li, H. Guo, P. Yue, X. Xiong, Z. He and Q. Zhang, *Electrochim. Acta*, 78 (2012) 331.

24. G.-Q. Zhang, W. Li, H. Yang, Y. Wang, S. B. Rapole, Y. Cao, C. Zheng, K. Ding and Z. Guo, *J. New Mat. Electr. Sys.*, 16 (2013)25.
25. Y. Wang, Z.-S. Feng, J. Hu, L. Yu, J.-J. Chen, L.-L. Wang, X.-J. Wang, H.-L. Tang, *Electrochim. Acta*, 117 (2014) 431.
26. C. Lin, B. Ding, Y. Xin, F. Cheng, M. O. Lai, L. Lu and H. Zhou, *J. Power Sources*, 248 (2014) 1034.
27. K. Ding, H. Gu, C. Zheng, L. Liu, L. Liu, X. Yan and Z. Guo, *Electrochim. Acta* , 146 (2014) 585.
28. K. Ding, Y. Zhao, L. Liu, Y. Li, L. Liu, L. Wang, X. He and Z. Guo, *Electrochim. Acta*, 176 (2015) 240.
29. K. Ding, T. Okajima and T. Ohsaka, *Electrochemistry*, 75 (2007) 35.
30. M. Guo, S. Wang, L.-X. Ding, C. Huang and H. Wang, *J. Power Sources*, 283 (2015) 372.
31. Y. H. Rho and K. Kanamura, *J. Solid State Chem.*, 177 (2004) 2094.

© 2016 The Authors. Published by ESG ([www.electrochemsci.org](http://www.electrochemsci.org)). This article is an open access article distributed under the terms and conditions of the Creative Commons Attribution license (<http://creativecommons.org/licenses/by/4.0/>).